

Escherichia coli Hfq has distinct interaction surfaces for DsrA, *rpoS* and poly(A) RNAs

Peter J Mikulecky¹, Meenakshi K Kaw², Cristin C Brescia², Jennifer C Takach¹, Darren D Sledjeski² & Andrew L Feig¹

The bacterial Sm-like protein Hfq facilitates RNA-RNA interactions involved in post-transcriptional regulation of the stress response. Specifically, Hfq helps pair noncoding RNAs (ncRNAs) with complementary regions of target mRNAs. To probe the mechanism of this pairing, we generated a series of Hfq mutants and measured their affinity for RNAs like those with which Hfq must associate *in vivo*. We tested the mutants' DsrA-dependent activation of *rpoS*, and their ability to stabilize DsrA ncRNA against degradation *in vivo*. Our results suggest that Hfq has two independent RNA-binding surfaces. In addition to a well-known site around the core of the Hfq hexamer, we observe interactions with the distal face of Hfq, a new locus with which mRNAs and poly(A) sequences associate. Our model explains how Hfq can simultaneously bind a ncRNA and its mRNA target to facilitate the strand displacement reaction required for Hfq-dependent translational regulation.

Hfq protein from *Escherichia coli* was first described in connection with Q β -phage replication^{1,2}. Hfq has recently emerged as a central player in post-transcriptional gene regulation as mediated by bacterial ncRNAs^{3–6}. *Escherichia coli* Hfq mutants show disrupted signaling in stress response pathways^{7,8}, arising from the need for Hfq to mediate base-pairing between regulatory ncRNAs and their mRNA targets. Examples of these partnerships include DsrA-*rpoS*^{7,9,10}, OxyS-*fhfA*^{11,12}, OxyS-*rpoS*¹³, RprA-*rpoS*¹⁴, RyhB-*sodB*^{15–17} and Spot42-*galETKM*¹⁸.

Complexes between ncRNAs and their mRNA targets function in several ways. Most commonly, complexed structures lead to translational activation or repression by remodeling mRNA regulatory regions containing the ribosome-binding site (RBS) and/or start codon. Alternatively, the interaction can enhance decay of the target mRNA¹⁶ or simply block translation¹¹. Clearly, Hfq facilitates base-pairing between ncRNAs and their targets, but how it does so is poorly understood. How the chaperone function relates to other Hfq activities such as the control of poly(A) tail elongation^{19,20} and regulation of mRNA stability^{21,22} is also unknown.

Hfq shares sequence similarity to the eukaryotic Lsm proteins^{23–27}. In the Conserved Domain Database²⁸ Hfq is listed under the Sm and Sm-like protein family as well as among the eubacterial Hfqs. An alignment of the conserved Lsm and Hfq motifs shows that the Sm1 and Sm2 regions overlap with the Hfq motif (Fig. 1). Crystallographic characterization of Hfq revealed a classical Sm fold, as predicted from sequence alignment and homology modeling^{27,29}. Whereas eukaryotic Sm proteins form heteroheptameric rings^{30–32}, Hfq forms homoheptamers similar to the archaeal Sm proteins^{33,34}. RNA-binding contacts are observed for both Hfq and Sm proteins in cocrystal struc-

tures with short (A+U)-rich oligonucleotides, and show that these small RNA substrates interact with their protein partners in a similar manner (Fig. 1).

Two parallel but nonexclusive models have been proposed to explain how Hfq promotes intermolecular base-pairing. In the first model, Hfq acts explicitly as an RNA chaperone, partially unfolding one or both RNAs^{35,36}. In the second model, Hfq binds both RNAs, increasing their local concentration to induce the interaction. Several studies have probed RNA structural changes upon Hfq binding. DsrA ncRNA showed no substantial secondary structure changes³⁷. The *rpoS* mRNA 5' untranslated region (5' UTR) was not assayed for structural changes in this study, but more recent work indicates that the *rpoS* leader sequence also remains unchanged upon binding Hfq (R. Lease and S. Woodson, Johns Hopkins University, personal communication).

Several studies suggested that more than one RNA can simultaneously assemble onto Hfq. Work by two groups has recently shown that stable ternary complexes containing DsrA, *rpoS* mRNA and Hfq can form (P.J.M., E. Espinosa, Indiana University, and A.L.F., unpublished data; R. Lease and S. Woodson, Johns Hopkins University, personal communication). These complexes represent product-like states wherein the two RNAs are already base-paired with one another on Hfq. Similar ternary complexes have been observed in coimmunoprecipitation experiments²⁵. It seems possible, therefore, that the single RNA-binding site observed crystallographically is not sufficient for Hfq's ability to promote intermolecular base-pairing.

We addressed these questions through a mutational analysis of Hfq, probing *in vitro* binding to several model RNAs that represent species with which Hfq must interact. Hfq mutants were assayed *in vivo* using a reporter assay and RNA lifetime experiments. Together, the results

¹Department of Chemistry, Indiana University, 800 E. Kirkwood Avenue, Bloomington, Indiana 47405, USA. ²Department of Microbiology and Immunology, Medical College of Ohio, Toledo, 3055 Arlington Avenue, Ohio 43614-5806, USA. Correspondence should be addressed to A.L.F. (afeig@indiana.edu).

Published online 7 November 2004; doi:10.1038/nsmb858

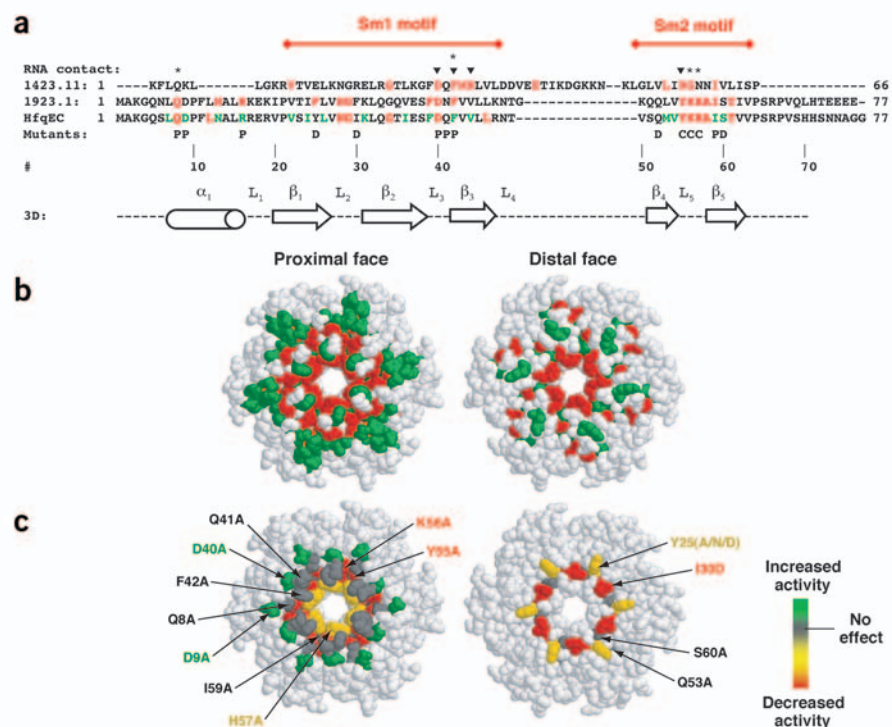


Figure 1 Sequence alignments and structure of Hfq. **(a)** Sequences 1412.11 and 1923.1 are entries from the conserved domain database representing the superfamily of Lsm proteins and Hfq, respectively. The two conserved domains have been aligned to properly juxtapose the motifs present in both protein families. Sequence elements in red represent the most highly conserved portions of the domain. HfqEC is the *E. coli* Hfq protein, colored based on an alignment of 25 bacterial Hfq homologs showing complete identity and sequence similarity in red and green, respectively. Above the alignment, triangles mark sites where RNA is known to interact with Lsm proteins and diamonds indicate known RNA-binding interactions with Hfq. The bottom line of the alignment shows the sites mutated as part of the study; P, location on the proximal face; D, location on the distal face; C, central cavity mutation. Numbering is provided for reference and is based on the *E. coli* Hfq sequence. Secondary structure information derives from the crystal structure of HfqEC (PDB entry 1HK9)²⁷. **(b)** Space-filling representation of the HfqEC crystal structure (PDB entry 1HK9) color-coded with the sequence conservation data from the HfqEC alignment in **a**. The distal face representation shows the same image rotated 180° relative to the proximal face around a vertical axis in the plane of the page. **(c)** Space-filling representation of the HfqEC crystal structure upon which the composite RNA binding data from **Table 1** have been superimposed.

Hfq I30D, Hfq Q53A and Hfq S60A mutations represent sites on the distal face of the Hfq hexamer. All mutants were expressed as His₆-tag fusion proteins. In control experiments, the His₆-tag had no substantial effect on the binding properties of Hfq *in vitro* (as assayed by gel shift and calorimetry) and His₆-tagged Hfq fully complements an *hfq*⁻ strain *in vivo*.

RNA-binding properties of mutant Hfqs

Previous data from our labs suggested that two or more RNA-binding surfaces might be present on Hfq³⁷. When poly(A) was used in an attempt to compete away DsrA in a gel shift assay, a supershift was observed rather than competitive binding³⁷. Therefore, to assess the effect of these mutations on RNA binding, several different RNA substrates were tested, including DsrA, RNA-U (a 7-nucleotide (nt) RNA with the sequence AU₅G), *rpoS* mRNA 5' UTR and A₂₇ (a 27-nt synthetic poly(A) oligomer). DsrA and RNA-U represent the ncRNAs, all of which contain (A+U)-rich sequences as part of their minimal binding element. This comparison is reinforced by the fact that short poly(U) RNAs have been shown to supplant DsrA in competitive binding experiments³⁷. *rpoS* mRNA 5' UTR and A₂₇ represent the target mRNAs regulated by the ncRNA, corresponding to the 5' and 3' termini of the mRNA, respectively.

RNA binding was probed using gel mobility shift assays and isothermal titration calorimetry. In the case of DsrA, the RNA shifts, and then supershifts, as it binds first one then a second equivalent of Hfq hexamer (**Fig. 2a**). The *rpoS* mRNA 5' UTR construct that we used also probably binds at least two equivalents of the Hfq hexamer. Because the initial species never accumulates significantly we have treated the *rpoS* mRNA-binding data as a single transition providing an apparent K_d (**Fig. 2b**).

support a model wherein at least two independent RNA-binding sites exist on the Hfq hexamer, and juxtaposition of bound RNAs facilitates base-pairing.

RESULTS

Hfq mutagenesis

To identify amino acids essential for RNA binding, we constructed a series of *E. coli* Hfq missense mutants (**Fig. 1**). Hfq Y55A, Hfq K56A and Hfq H57A contain mutations that cluster around the central cavity of the hexamer, a region that interacts with short (A+U)-rich sequences in the Hfq-RNA cocrystal structure²⁹. Other mutants, such as Hfq D40A, Hfq Q41A and Hfq F42A lie along the proximal surface of the torus. Minimal binding site studies have shown that Hfq preferentially binds (A+U)-rich sequences adjacent to double-stranded regions^{37,38}. Thus, these sites represent a potential contact surface for the duplex were it to lay down onto Hfq adjacent to the site at which the (A+U)-rich sequence binds. Hfq Q8A and Hfq D9A represent a series of highly conserved residues that lie on the proximal face of the torus that might contact RNAs a bit farther from the central cavity. Finally, the Hfq Y25A, Hfq Y25N, Hfq Y25D,

We consolidated the data from the 4 RNA substrates for each mutant Hfq, represented as the $\Delta\Delta G$ relative to binding wild-type Hfq (**Fig. 2c**). DsrA binds to wild-type Hfq with an affinity of 21 ± 1 nM (reported as hexamer, 126 nM monomer). Under the same conditions, the second binding event occurs with a K_d of 94 nM (reported as hexamer, 564 nM monomer). This value is within two-fold of those previously determined³⁷. DsrA affinity is affected by residual RNA often found to copurify with Hfq. The RNase A treatment in the current purification significantly reduced residual RNA and is probably the origin of the tighter affinities measured here.

Most of the mutations had relatively small effects on DsrA-binding affinity (**Table 1**), the largest being on the order of 20-fold decreased affinity, corresponding to a $\Delta\Delta G$ of ~ 1.8 kcal mol⁻¹. The modest effects of the point mutants could have resulted from polyvalent interaction between the larger RNAs and Hfq masking defects in one of the binding domains³⁷. If this were true, the smaller RNAs (RNA-U and A₂₇) would provide a more sensitive gauge of whether the residue participates in the RNA-protein interaction.

Under the same gel conditions, RNA-U exhibits poor affinity for the wild-type Hfq hexamer (2.5 ± 0.2 μ M hexamer, 15 μ M monomer).

Table 1 Comparison of *in vitro* affinity data with *in vivo* activities for Hfq mutants

Mutant	K_d (nM hexamer)				Hfq accum.	<i>rpoS::lacZ</i> assay	DsrA $t_{1/2}$ (min)
	DsrA ^a	RNA-U	<i>RpoS</i> mRNA 5' UTR	A ₂₇			
Wild type	21 ± 1 94 ± 5	2,500 ± 200	49 ± 1	39 ± 1	Yes	5.7 ± 0.7	55 ± 3 ^b
Q8A	19 ± 1 48 ± 2	2,400 ± 100	27 ± 1	24 ± 1	Yes	3.2 ± 0.2	–
D9A	14 ± 1 56 ± 1	320 ± 40	35 ± 2	36 ± 1	Yes	7 ± 1	–
Y25A	19 ± 1 35 ± 1	–	32 ± 1	196 ± 3	Yes	–	–
Y25N	15 ± 1 37 ± 2	–	24 ± 1	229 ± 2	Yes	4.5 ± 0.6	–
Y25D	16 ± 1 38 ± 1	–	22 ± 1	224 ± 2	Yes	4.0 ± 0.9	–
I30D	26 ± 1 41 ± 2	–	35 ± 1	363 ± 3	Yes	5.2 ± 0.9	–
D40A	27 ± 1 88 ± 2	760 ± 90	46 ± 1	36 ± 1	No	0.8 ± 0.1	–
Q41A	25 ± 1 98 ± 4	2,100 ± 100	70 ± 2	26 ± 1	Yes	6.4 ± 0.9	–
F42A	31 ± 1 95 ± 4	3,500 ± 300	50 ± 1	40 ± 1	Impaired	2.5 ± 0.2	–
Q53A	–	–	–	–	Yes	3.0 ± 0.6	–
Y55A	82 ± 4 1,600 ± 100	>20,000	82 ± 3	115 ± 2	Yes	0.8 ± 0.1	29 ± 5
Y55W	47 ± 1 121 ± 8	>10,000	45 ± 1	69 ± 1	Yes	4.5 ± 0.8	–
K56A	101 ± 2 224 ± 9	>20,000	104 ± 3	59 ± 1	Yes	1.0 ± 0.2	0.9 ± 0.1 ^c
H57A	44 ± 1 108 ± 3	>20,000	53 ± 1	55 ± 1	Yes	5.4 ± 0.5	–
I59A	–	–	–	–	Yes	4.2 ± 0.5	–
S60A	–	–	–	–	Yes	5.0 ± 0.3	–
Y25D Y55A	194 ± 9 ^d	>20,000	206 ± 6	270 ± 12	–	–	–
Y25D Y55W	34 ± 1 106 ± 7	>10,000	54 ± 1	400 ± 4	–	–	–
Y25D K56A	84 ± 3 320 ± 24	>60,000	77 ± 2	177 ± 3	–	–	–
I30D Y55A	190 ± 34 ^d	>20,000	270 ± 22	590 ± 11	–	–	–
I30D Y55W	41 ± 12 110 ± 13	>20,000	55 ± 1	312 ± 9	–	–	–
I30D K56A	52 ± 1 190 ± 19	>60,000	71 ± 2	280 ± 10	–	–	–

^aDsrA exhibits two sequential transitions—a shift and a supershift. The first value corresponds to K_1 and the second value to the supershift, K_2 . Close inspection of the *rpoS* mRNA 5'-UTR shifts reveals two apparent shifted species similar to those seen with DsrA. However, the two transitions are sufficiently coupled that they cannot be fit separately. ^b*Hfq*[−] strains have a DsrA $t_{1/2}$ of 5 ± 2 min. ^cThese data show a biphasic time dependence. A total of 90% of the DsrA RNA decays with a $t_{1/2}$ of 0.9 min. The final 10% of the RNA shows a much longer $t_{1/2}$, ~35 min. ^dNo clear distinction between K_1 and K_2 behavior was possible owing to abnormal smearing of the bands. Data were fit to a single transition.

This result is consistent with minimal binding studies that have shown Hfq preferentially binds (A+U)-rich sequences adjacent to base-paired elements³⁷. Despite the weak interactions, binding is perturbed by specific mutations. Hfq D9A showed eight-fold tighter binding to RNA-U. Mutant proteins Hfq Y55A, Hfq Y55W, Hfq K56A and Hfq H57A were

sufficiently defective that no binding was observed, even at the highest protein concentrations.

Because RNA-U bound so weakly, we compared its affinity to those of a pair of RNAs that should not specifically bind Hfq—the substrate and ribozyme strands of hammerhead ribozyme 16 (ref. 39). These

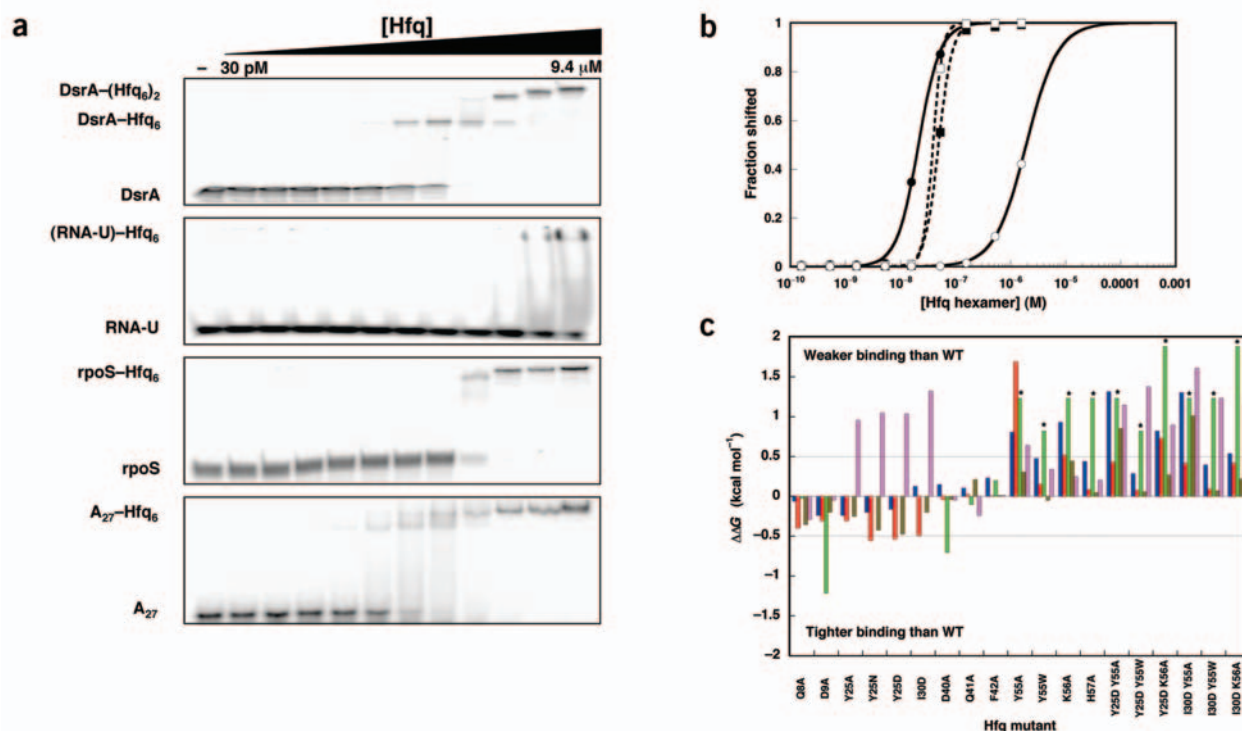


Figure 2 *In vitro* analysis of RNA binding to mutant Hfq proteins. (a) Gel shift experiments showing the binding of wild-type Hfq to DsrA, RNA-U, *rpoS* mRNA 5' UTR and A₂₇. (b) Quantification of the gel shift experiments in a. (c) Quantification of the gel shift experiments in a. Closed circles, DsrA K₁; open circles, RNA-U; closed squares, *rpoS* mRNA 5' UTR; open squares, A₂₇. Lines represent nonlinear least-squares fitting to a cooperative binding model. (c) Histogram showing the free energy of binding relative to wild-type (WT) Hfq for each Hfq mutant. ΔΔGs between -0.5 and 0.5 kcal mol⁻¹ indicate insignificant effects on RNA binding. Asterisks indicate data that are lower limits of the actual effect as the interactions were too weak to be measured. Blue, DsrA-Hfq₆; red, DsrA-(Hfq₆)₂; green, RNA-U; brown, *rpoS* mRNA 5' UTR; lavender, A₂₇.

RNAs showed no gel shift behavior up to 30 μM Hfq monomer. The interaction of RNA-U with the mutant Hfqs clearly approaches that of pure nonspecific binding under these conditions. At the same time, the deleterious effects of mutations within the Sm2 core motif suggest that RNA-U binding occurs at the crystallographically observed site.

With respect to *rpoS* mRNA 5' UTR binding, the collection of mutations we prepared showed few effects. The largest defect observed across the series, with Hfq K56A, was only two-fold. This result indicates that perhaps not all RNAs bind via the central core and the Sm2 motif. Distal face mutations also did not significantly affect *rpoS* mRNA 5'-UTR binding. Two double mutants (Hfq Y25D Y55A and Hfq I30D Y55A) that combine defects in the Sm2 motif with those on the distal face show reduced affinity for *rpoS* mRNA 5' UTR, however. These data suggest that *rpoS* mRNA 5' UTR may interact with both faces of Hfq.

Very different results were observed in the case of A₂₇ binding. Gel shift experiments measured an affinity of 39 ± 1 nM for wild-type Hfq hexamer (234 nM in monomer). Of the proximal face mutants, the most impaired was Hfq Y55A, but this protein had only a three-fold effect on binding. These results suggest that the Sm2 region at the center of the torus does not interact in any significant way with A₂₇ and is consistent with the additive binding behavior previously observed between DsrA domain II and poly(A)³⁷. The distal face mutants showed different behavior, however. Mutations at Tyr25 and Ile30 affected A₂₇ binding, leading to a ten-fold loss in affinity for Hfq Y25D and Hfq I30D. Double mutants showed no additional changes in affinity for A₂₇ when Sm2 motif changes were combined with distal face mutations. We therefore infer that poly(A) interacts with the distal face of Hfq.

Competition experiments reveal two independent binding sites

Previous experiments with wild-type Hfq showed what seemed to be mutual binding of A₂₇ and DsrA to Hfq³⁷. In light of the results described above, we carried out a series of competition experiments using gel shift assays to look at the effect of A₂₇ addition to binary complexes containing either DsrA or *rpoS* mRNA 5' UTR prebound to Hfq (Fig. 3 and Table 2). We observed markedly different behavior for wild-type Hfq, Hfq Y25D and Hfq K56A. Concomitant binding of A₂₇ and either DsrA or *rpoS* mRNA 5' UTR was observed at concentrations of wild-type Hfq sufficient to promote the formation of the DsrA-(Hfq₆)₂ species, consistent with our previous findings³⁷. When the distal face mutant Hfq Y25D was used, additive binding was completely abolished, indicating that A₂₇ binding was independent of DsrA and *rpoS* mRNA 5' UTR (data not shown). When the Sm2 mutant Hfq K56A was used, a third outcome resulted. The addition of A₂₇ displaced DsrA; it similarly displaced *rpoS* mRNA 5' UTR, albeit less efficiently. The band resulting from DsrA displacement by A₂₇ migrated more slowly in the native gel than unbound DsrA, with mobility similar to that of DsrA dimer (data not shown).

The competition experiments lead to two conclusions. First, Hfq K56A binds DsrA improperly, allowing for competition by A₂₇. Second, this abnormal binding mode possibly leads to altered folding of the ncRNA and assembly of DsrA dimers—a trait that could lead to adverse consequences *in vivo*.

Isothermal titration calorimetry

An alternative way to measure Hfq-RNA interactions is with isothermal titration calorimetry (ITC)^{40–42}. This method offers several advan-

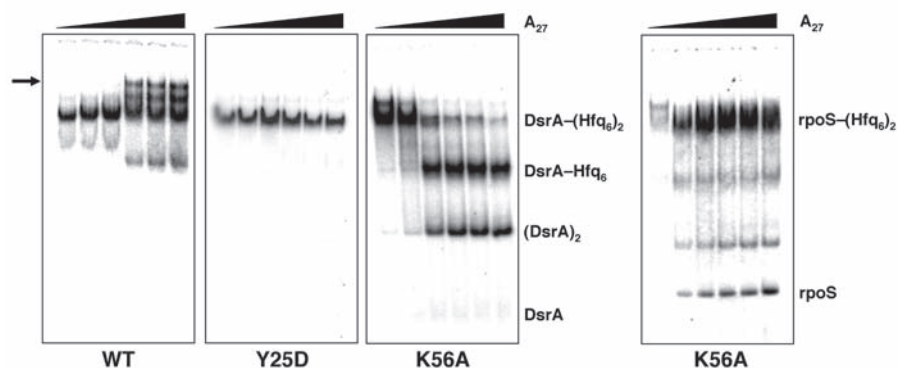


Figure 3 Native gel analysis showing the effect of A_{27} addition to the DsrA-(Hfq₆)₂ complex. DsrA-(Hfq₆)₂ was preassembled at appropriate concentrations of Hfq (based on the measured affinity constants in **Table 2**) using ³²P-labeled DsrA before the addition of unlabeled A_{27} (0, 0.03, 0.1, 0.3, 1 or 3 μ M). Gels compare the behavior of wild-type (WT) Hfq to Hfq Y25D and Hfq K56A as labeled. A supershifted species is observed (arrow) only in the case of WT Hfq. For Hfq Y25D, the addition of A_{27} had no effect on DsrA binding. For Hfq K56A, A_{27} displaced DsrA in the form of the homodimer, DsrA₂, based on its gel migration against authentic standards.

tages over the gel shift experiments. Reaction stoichiometry is more readily determined from the data. Furthermore, detailed thermodynamic information is obtained more accurately than from electrophoretic methods, because the enthalpic contribution of the free energy is measured directly.

A typical ITC experiment is shown in **Supplementary Figure 1** online. Consistent with the gel shift experiments, DsrA, *rpoS* mRNA 5' UTR and poly(A) showed tight binding to Hfq hexamer with K_d values in the low nanomolar range. Because of the weak interaction between Hfq and RNA-U (~2.5 μ M from gel shift analysis), we could not achieve the necessary sample concentrations to study its binding accurately using this method. Hfq Y55A showed a 50-fold reduction in binding affinity whereas the Hfq K56A showed a 30-fold reduction in binding affinity for DsrA, whereas Hfq H57A had nearly wild-type affinity. Both results are consistent with the gel shift experiments (**Supplementary Table 1** online).

The apparent stoichiometries from the ITC experiments are consistent with Hfq acting as a preformed hexamer and binding a single equivalent of DsrA or *rpoS* mRNA 5' UTR. Thus, the ITC data imply that the binding of a second equivalent of Hfq to an RNA (K_2) may result from working under trace RNA conditions, as typically done in gel shift assays. An unexpected result was observed in poly(A) experiments, however. Fitting of the ITC data suggests that A_{18} (a shorter, 18-nt poly(A) RNA was used in these experiments to diminish the likelihood that multiple Hfqs might bind to the longer RNA⁴³) binds two identical sites per Hfq hexamer.

Binding enthalpies (ΔH°) of -40 to -80 kcal mol⁻¹ were measured for the same three substrates with corresponding binding entropies (ΔS°) of -100 to -250 cal mol⁻¹ K⁻¹ (**Supplementary Table 1** online). These values show that the enthalpy of the interaction is quite favorable, but largely offset by highly unfavorable entropy. As these parameters combine the energetic contribution of the binding phenomenon with any potential RNA rearrangements, a detailed interpretation requires further study.

Accumulation and complementation analysis of Hfq mutants

Within a living cell, the interaction of Hfq with mRNAs and ncRNAs is much more complex than that probed with our *in vitro* model system. To determine whether the Hfq mutants function *in vivo* we used an

rpoS::lacZ reporter system in an *hfq*⁻ strain of *E. coli* (**Fig. 4**)⁷. Expression of this reporter requires both transcription and translation of *rpoS*⁷. The assay tests for two phenomena. First, plasmid-borne mutant Hfqs must accumulate, and second, they must facilitate proper post-transcriptional regulation of *rpoS*. Because DsrA is the predominant ncRNA involved in the translational regulation of *rpoS* at low temperatures, all assays were conducted at 30 °C (ref. 44). To prevent overexpression of Hfq, the mutants were expressed under control of the inducible *araBAD* promoter⁴⁵. In agreement with previous work⁷, in the absence of arabinose or with vector alone, very little Hfq accumulated (**Fig. 4b**) and RpoS::LacZ expression was low (**Fig. 4c**). Addition of 150 μ M arabinose induced wild-type expression levels of Hfq and normal translation of RpoS::LacZ (**Fig. 4c**).

As misfolded proteins tend to be degraded and cleared from the cell, western blotting was used to ensure that mutant Hfqs accumulated

normally at the same arabinose concentration. Most of the mutants provided normal expression under these conditions, as can be seen for representative mutants like Hfq Y55A and Hfq K56A. Hfq D40A and Hfq F42A (**Fig. 4b**, lanes 6 and 7) showed abnormal accumulation, however. Circular dichroism (CD) and dynamic light scattering verified that these proteins fold and hexamerize *in vitro*, but they may be sufficiently destabilized to pose a problem *in vivo*. Because there was a significant decrease in the Hfq concentration in these cells, any loss of activity in the reporter complementation assay (**Fig. 4c**) could result from either defective RNA binding or decreased protein accumulation.

As expected from the *in vitro* experiments, Hfqs containing mutations in the Sm2 motif, including Hfq Y55A and Hfq K56A, did not complement the *hfq*⁻ phenotype. As these proteins were present at wild-type levels based on western blot analysis, these results suggest that loss of *in vivo* activity for these mutants was not due to decreased accumulation. Notably, Hfq H57A and Hfq Y55W, mutants that do not bind RNA-U but retain wild-type DsrA and *rpoS* mRNA 5' UTR affinity *in vitro*, retained their *in vivo* activity. This finding suggests that the small changes in DsrA binding observed *in vitro* for Hfq Y55A and Hfq K56A are more diagnostic of the *in vivo* behavior than RNA-U binding. Other mutations within the phylogenetically conserved Sm2 region showed no defects in our assay.

Table 2 Summary of A_{27} competition experiments

Complex	Mutant	[Hfq] (nM hexamer)	Outcome upon A_{27} competition
DsrA-Hfq ₆	Wild type	42	No effect
	Y25D	25	No effect
	K56A	125	Abnormal competition
DsrA-(Hfq ₆) ₂	Wild type	125	Supershift
	Y25D	83	No effect
	K56A	250	Abnormal competition
<i>rpoS</i> -(Hfq ₆) ₂	Wild type	83	Supershift
	Y25D	50	No effect
	K56A	125	No effect

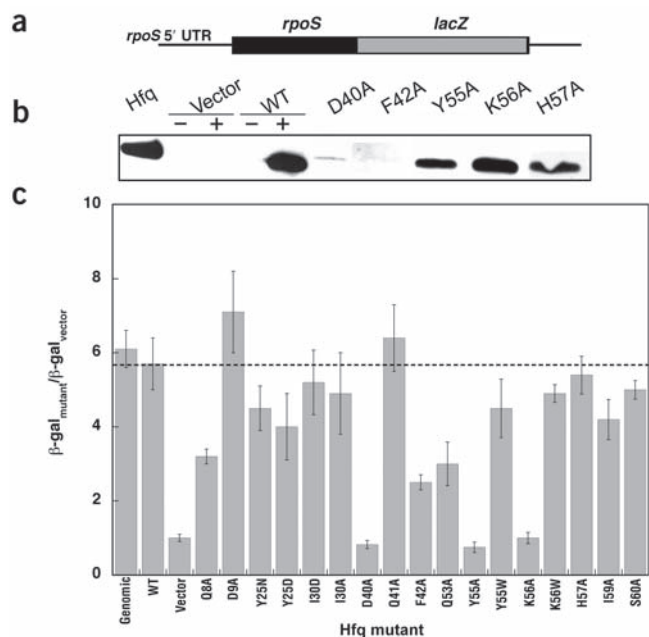


Figure 4 Assay for *in vivo* accumulation and *rpoS* activation. **(a)** Schematic diagram of the reporter construct used for the Hfq complementation assay. **(b)** Western blot showing the accumulation of Hfq *in vivo*. In the control lanes, + and – refer to the presence or absence of 150 μM arabinose, added to induce Hfq from an *araBAD* promoter. Vector represents the pBAD plasmid⁴⁵ without the *hfq* gene. The Hfq lane shows the endogenous Hfq levels in an *hfq*⁺ strain of *E. coli*. **(c)** Histogram showing the results of *in vivo* translational activation of the RpoS::LacZ fusion protein for wild-type (WT) and mutant Hfq proteins. Values <4 are considered significant defects based on the error in this assay. β-gal, β-galactosidase activity.

Assessment of DsrA stability *in vivo*

RNA lifetime analysis has been used as another measure of Hfq activity *in vivo*^{7,16,38}. In the presence of Hfq, DsrA has been shown to degrade significantly more slowly than when Hfq is absent⁷. We measured DsrA lifetimes for both Hfq mutants that had significantly reduced activity in complementation assays that could not be explained by simple accumulation defects. Hfq Y55A and Hfq K56A show markedly different behavior after inhibition of transcription with rifampicin (Fig. 5). Whereas Hfq Y55A led to long-lived RNA similar to wild-type Hfq, in the presence of Hfq K56A, DsrA degraded rapidly. The behavior occurred with biphasic kinetics. DsrA degraded in the fast phase, accounting for ~90% of the total, was less stable than in the absence of Hfq entirely. The remaining 10% of the RNA was reasonably long-lived.

DISCUSSION

Site-directed mutagenesis was used to probe the interaction between Hfq and four RNAs that represent some of the ncRNAs and mRNAs with which Hfq interacts *in vivo*. The effects of these mutations were assayed both *in vitro* and *in vivo*. Sites of mutation were chosen based on structural and phylogenetic information. Structurally, we can group the mutants into three categories: those affecting the central cavity (Y55A, K56A and H57A), the proximal face (Q8A, D9A, D40A, Q41A, F42A and I59A) or the distal face (Y25X, I30X, Q53A and S60A). Notably, mutations at these loci had distinct effects on behavior, both *in vitro* and *in vivo*.

Two central cavity mutations severely impair function

Previous studies had implicated the central cavity as essential for Hfq and Sm protein function. Only two cavity mutants, Hfq Y55A and Hfq K56A, showed consistent *in vitro* defects in binding to DsrA. Both mutations target highly conserved residues within the Sm2 motif. Mutations

at other conserved Sm2 residues (His57, Ile59 and Ser60) did not significantly impair *in vitro* or *in vivo* behavior.

The minimal substrate RNA-U showed much greater sensitivity to Sm2 region mutations, whereas *rpoS* mRNA 5' UTR and A₂₇ were unaffected. The known RNA-binding cavity along the inner rim of the Hfq hexamer thus seems only to interact with the (A+U)-rich elements of the ncRNAs, and does not represent the primary binding surface for poly(A) sequences or mRNAs. Additional RNA-binding surfaces must be present on Hfq, supporting the idea that Hfq functions by colocalizing ncRNAs and their mRNA targets. Hfq probably facilitates the strand exchange reaction largely by putting the RNAs in close proximity, and possibly by presenting appropriate interaction surfaces toward one another.

The DsrA half-life experiments provide an additional window into the complexities of the Hfq system. Previous work has shown that in the absence of Hfq DsrA stability is markedly decreased *in vivo*⁷. This effect is thought to be due to the overlap of the Hfq-binding and RNase E cleavage sites on DsrA. Although both Hfq Y55A and Hfq K56A are inactive for DsrA-mediated regulation of *rpoS*, their abilities to stabilize DsrA *in vivo* are diametrically opposed. Hfq Y55A behaves like wild-type Hfq whereas Hfq K56A provides DsrA almost no protection from RNase E. The notable ability of Hfq Y55A to stabilize DsrA suggests that, although DsrA binds to Hfq Y55A *in vivo*, it cannot correctly interact with *rpoS* mRNA. This difference between Hfq Y55A and Hfq K56A could relate to the stability of a ternary complex involving Hfq, DsrA and *rpoS* mRNA (P.J.M., E. Espinosa, Indiana University, and A.L.F., unpublished data).

Proximal face mutations show few specific effects

Most of the proximal face mutations showed little effect on *in vitro* and *in vivo* activity. Where disagreement was observed (Hfq D40A and Hfq F42A), the data are rectified by protein accumulation defects *in vivo*. Although it is unclear why these two mutants fail to accumulate, the result clearly explains their inability to complement the *hfq*⁻ strain.

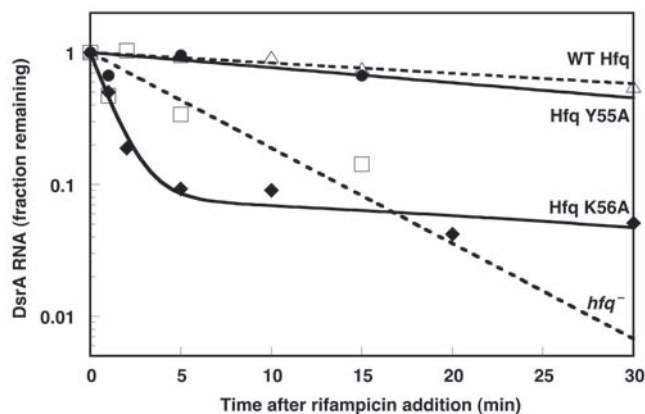


Figure 5 Lifetime analysis of DsrA *in vivo*. Data are based on QRT-PCR for wild-type (WT) Hfq and selected mutants using primers specific for full-length DsrA. Solid lines (Hfq mutants) and dashed lines (Hfq and *hfq*⁻) are least-squares fits to the data from which the half-lives were calculated. Hfq K56A has been fit to a double-exponential decay whereas the other data are fit to a single-exponential model.

Distal face mutations alter binding only to poly(A)

Distal face mutants were generated to test the hypothesis that RNA- or protein-binding interactions might occur on that face^{5,37}. Hfq Y25D and Hfq I30D bound A₂₇ with five- to ten-fold reduced affinity, but did not show altered binding to any of the other three RNA substrates.

The distal face mutants complemented the *rpoS* activation function of wild-type Hfq *in vivo*, and effectively bound DsrA and *rpoS* mRNA 5' UTR *in vitro*. Hfq is known to be involved in modulating polyadenylation, however. Because all mutations that altered poly(A) binding localized to the distal face, one might infer that polyadenylation control uses this surface of the protein. Further studies are required to find whether these mutations differentially affect polyadenylation.

Archaeal Sm proteins are believed to aggregate into long rodlike structures⁴⁶. Even in the absence of extended rods, a dodecameric structure could have explained well how Hfq hexamers bring together RNAs in a pairwise fashion. Such a model requires the distal face to be involved in an Hfq-Hfq contact. The addition of six aspartates in lieu of hydrophobic residues at this potential interaction surface should have been quite destabilizing were such face-to-face dodecamerization important. Our results do not absolutely preclude the formation of such species, but they do argue against it.

rpoS mRNA 5'-UTR binding remains mysterious

An unresolved issue from this work is where *rpoS* mRNA binds Hfq. The work of Lease and Woodson indicates that several U-rich sequences within the *rpoS* mRNA 5' UTR become protected from nuclease digestion upon Hfq binding (R. Lease and S. Woodson, Johns Hopkins University, personal communication). Such results imply an interaction with the central cavity, but our data suggest that, if the mRNA binds the central cavity, additional contacts must mask effects of the Y55A and K56A mutations. In addition to the 5' UTR used in these studies, *rpoS* mRNA *in vivo* would contain the coding region and the 3' UTR. Does the mRNA naturally contact both faces of Hfq? If so, additional binding determinants might be present along the exterior edge of the torus. Our current study has not probed those regions. Furthermore, the C-terminal extension of Hfq could contribute to RNA binding in ways we have not yet recognized.

Implications for understanding Sm and Lsm proteins

How do these data reflect on our understanding of the eukaryotic Sm and Lsm proteins, with which Hfq shares a common ancestor? In the *Pyrococcus abyssi* Sm1 core complex, RNA was shown to bind facially, near the end of strand β 2 (ref. 47), and binding was significantly impaired in a Y34V mutant. This binding surface corresponds to the L3 region in the Sm1 motif of Hfq, adjacent to Asp40, Gln41 and Phe42. Although the mutations at these sites do not exhibit the marked RNA-binding defect seen in the *P. abyssi* Sm1 system, the accumulation defect of Hfq D40A implies that this region along the proximal face of the torus is still critical for function of the resulting RNP complex. The eukaryotic SmG protein uses this L3 region to contact RNAs in spliceosomal small nuclear ribonucleoprotein (snRNP) cores^{48,49}. Our data are consistent with a second site of contact between the RNAs and Hfq, but the exact location of the L3 contacts may have evolved after the homohexameric Hfq complex diverged to form the heteromeric aggregates observed in modern spliceosomes. Current models of U1 snRNPs also imply significant contact between the duplex regions of the RNA and the outer rim of the torus. Further exploration will probe these surfaces.

In summary, these experiments reveal that Hfq contains at least two distinct RNA-binding surfaces. Mutations that alter ncRNA binding affinity cluster around the Sm2 domain, but do not significantly perturb affinity for *rpoS* mRNA 5' UTR. Additionally, distal face mutations

are the only ones tested that affect A₂₇ binding. Poly(A) RNA binding therefore uses contacts on the back face of the torus. Such an organization could spatially and functionally separate Hfq's effects on polyadenylation from those mediating base-pairing between ncRNAs and their mRNA targets.

METHODS

Plasmid construction for *rpoS* mRNA 5' UTR. The 5' UTR from *E. coli rpoS* (nucleotides -134 to +3) was obtained by PCR using the primers rpoSA1 and rpoSA2 (Supplementary Table 2 online) using Pfu Turbo (Stratagene). The PCR product was ligated into pUC19 using BamHI and EcoRI. The resulting DNA was transformed into XL-10 Gold cells (Stratagene). Plasmid pJEF-10301 was isolated by miniprep (Qiagen) and sequenced. Large-scale isolation of plasmid DNA was done using the Qiagen Gigaprep protocol, and the vector was prepared for runoff transcription by exhaustive digestion with SspI.

RNA preparation for *in vitro* binding. RNA-U, A₁₈ and A₂₇ were purchased from Dharmacon Research and deprotected following the manufacturer's protocol. RNA quality was assessed by denaturing PAGE and gel-purified as necessary. Other RNAs (DsrA and *rpoS* mRNA 5' UTR) were transcribed *in vitro* and gel-purified as described³⁷.

Site-directed mutagenesis. Using the QuikChange procedure (Stratagene), all mutants were prepared in two separate backgrounds. The pET-21b background has a C-terminal His₆-tag and was used for *in vitro* analysis. The pBAD24 background is under an arabinose promoter system and was used for *in vivo* analysis. All mutations were verified by sequencing.

Hfq expression and purification. Wild-type Hfq is heat-stable and the standard purification protocol exploits this property^{25,50}. As several of the mutant proteins were found to be heat-sensitive, all mutants (as well as wild-type Hfq) were purified by Co²⁺-affinity chromatography, using a C-terminal His₆-tag. Expression was induced by addition of 1 mM IPTG to cultures grown to A₆₀₀ = 0.4–0.6. Induction proceeded for 4 h at 37 °C before harvesting. Cell pellets (0.5-l equivalents) were resuspended in 25 ml lysis buffer (50 mM HEPES, pH 7.5, 500 mM NH₄Cl, 20 mM imidazole, 5% (w/v) glycerol) with EDTA-free Complete protease inhibitor cocktail (Stratagene) and lysed by ultrasonication. Lysate was treated with DNase I (100 U) and RNase A (100 μ g) and incubated on ice for 1 h. Centrifugally clarified lysate was passed over a Hi-trap metal chelation column (Amersham-Pharmacia) preloaded with CoSO₄. The column was washed with five volumes of lysis buffer, then five volumes of wash buffer 1 (50 mM HEPES, pH 7.5, 1 M NH₄Cl, 5% (w/v) glycerol). Hfq was eluted with five volumes of elution buffer 1 (50 mM HEPES, pH 7.5, 500 mM NH₄Cl, 250 mM imidazole, 5% (w/v) glycerol) followed by five volumes of elution buffer 2 (50 mM HEPES, pH 7.5, 8 M urea, 1 M NH₄Cl, 50 mM EDTA, 5% (w/v) glycerol). Protein was concentrated to 0.5–1.0 mg ml⁻¹ and dialyzed against storage buffer (50 mM HEPES, pH 7.5, 250 mM NH₄Cl, 1 mM EDTA, 10% (w/v) glycerol). Concentrations of protein and any residual RNA were assessed by the Warburg-Christian method⁵¹. Purity was assessed by SDS-PAGE. Mutants were checked by CD spectroscopy using a Jasco-J715 spectrometer and by dynamic light scattering using a Malvern Nano-S Zetasizer to ensure proper folding and oligomerization relative to wild-type Hfq.

Electrophoretic mobility shift assays. 5' end-labeled RNAs were annealed at 90 °C for 120 s, cooled to 37 °C, and incubated with Hfq for 30 min in 50 mM HEPES, pH 7.5, 250 mM NH₄Cl. Immediately before loading, samples were diluted with an equal volume of native loading buffer (10% (w/v) sucrose, xylene cyanol, bromophenol blue) or denaturing loading buffer (7 M urea, 1 \times TBE, xylene cyanol, bromophenol blue). Samples (15 μ l) were resolved at 5 W on either 5% (w/v) polyacrylamide native gels or 5% (w/v) polyacrylamide/7 M urea gels. Dried gels were visualized by phosphorimaging (Molecular Dynamics) using a Typhoon 9210 imaging system (Amersham-Pharmacia). Quantification was done using ImageQuant 5.2 (Molecular Dynamics) and Kaleidagraph 3.0 (Synergy). Data were fit using nonlinear least-squares analysis to a cooperative binding model. Cooperativity values (*n*) tended to fall between 2 and 3. Higher *n*-values yielded comparable goodness-of-fit parameters. In the case of the A₂₇ competition assays, complexes of DsrA or *rpoS* mRNA 5' UTR with Hfq were preassembled.

Isothermal titration calorimetry. Calorimetry was done on a MicroCal VP-ITC. Samples were dialyzed into reaction buffer (50 mM HEPES, pH 7.5, 250 mM NH₄Cl, 10% (w/v) glycerol) and degassed before loading each experiment. RNAs (21–25 μM) were titrated into 1.4 ml of 0.6–3.5 μM Hfq hexamer over 35 8-μl injections with constant stirring at 310 r.p.m., 4-min injection spacings, and thermostating at 25 °C. Data were corrected by subtraction of a baseline defined by the terminal 10–15 injection points after saturation of the binding event. Data were analyzed using Origin 7.0 (MicroCal) as described⁵².

Western blot analysis. Total cellular extracts of *E. coli* were separated on tris-tricine SDS 16% (w/v) polyacrylamide gels⁵³ and electroblotted⁵⁴ to PVDF membrane. Equal loading across lanes was verified by staining with Ponceau S (Sigma). The membrane was probed with rabbit anti-Hfq polyclonal anti-sera⁷. Antibody–antigen complex was visualized with goat anti-rabbit immunoglobulin horseradish-peroxidase-conjugated antibody (Pierce) and ECL reagent kit (Pierce).

Purification of RNA for half-life studies. DsrA half-life was determined as described^{37,55}. Cultures of wild-type and *hfq*⁻ strains were grown at 30 °C to A₆₀₀ = 0.4–0.6. Rifampicin (100 μg μl⁻¹ final concentration) was added and cells were collected at the indicated time points. These samples were added immediately to prechilled tubes containing 0.1 volume phenol stop solution (5% (v/v) buffered phenol, pH 7.4, in ethanol)⁵⁶. Cells were pelleted, resuspended in 200 μl TE (10 mM Tris, pH 8.0, 1 mM EDTA), and passed over QIAshredder mini columns (Qiagen). RNA was extracted with Trizol reagent (Invitrogen), precipitated with isopropanol, and washed with 75% (v/v) ethanol. RNA was incubated with 30 U of RQ1 DNase (Promega) at 37 °C for 20 min followed by DNase inactivation at 60 °C for 10 min. Trizol extraction and isopropanol precipitation were repeated before resuspension of RNA in RNase-free water. Concentrations were determined by measuring absorbance at 260 nm.

Quantitative RT-PCR (QRT-PCR). Relative RNA concentrations were determined by quantitative RT-PCR using a Roche LightCycler TaqMan PCR system (Applied Biosystems). Primer and probe design was based on the *E. coli* *dsrA* and 5S RNAs using Primer Express 1.5 (ABI). The *dsrA* primers and probes were designed to detect only full length DsrA. Primers and probes were chemically synthesized (IDT). Probes were 5' end-labeled with 6-carboxyfluorescein and 3' end-labeled with 'black hole quencher' BHQ1 (Biosearch Technologies). Each 10 μl RT-PCR mixture contained 50 ng RNA, LightCycler-RT-PCR reaction mix hybridization probe (Roche), LightCycler RT-PCR enzyme mix (omitted in RT-negative reactions), 300 nM each of the forward and reverse primers, and 250 nM Taqman probe. Both RT-positive and RT-negative reactions were tested in duplicate. Reactions were performed using a Roche LightCycler with optimized cycle conditions. DsrA RNA abundance relative to 5S ribosomal RNA was determined using the $-\Delta\Delta C_t$ method as described by the manufacturer (ABI). 5S RNA was used as the internal control.

In vivo RpoS::LacZ fusion activity. RpoS::LacZ fusion activity was determined as described⁷. Briefly, cells were grown at 30 °C in LB medium with the appropriate antibiotic. Total β-galactosidase units were determined as described⁵⁷ and plotted against the culture A₆₀₀. The slope of the linear regression (differential rate of expression) was used as the specific activity. Mutant activities were determined at least three times and s.d. calculated.

Note: Supplementary information is available on the Nature Structural & Molecular Biology website.

ACKNOWLEDGMENTS

This work is supported by grants from the US National Institutes of Health (GM065430 to A.L.F., GM056448 to D.S., and T32-GM07757 to Indiana University/P.J.M.). A.L.F. is a Cottrell Scholar of Research Corporation. The Typhoon 9210 imaging system was purchased with a grant from the US National Science Foundation (DBI-0244815). The authors thank T. Stone (Indiana University) for technical support in the Physical Biochemistry Instrumentation Facility, and J. Fitzgerald, A. Kerzmann, N. Anderson and S. Kamel (Indiana University) for assistance in the cloning and sequencing of the constructs.

COMPETING INTERESTS STATEMENT

The authors declare that they have no competing financial interests.

Received 1 July; accepted 30 September 2004

Published online at <http://www.nature.com/nsmb/>

- Hori, K. & Yanazaki, Y. Nucleotide sequence specific interaction of host factor I with bacteriophage Q β RNA. *FEBS Lett.* **43**, 20–22 (1974).
- Van Emmelo, J., De Boever, J., Gillis, E. & Fiers, W. A host factor required for Q-β-RNA-replication in "*Escherichia coli*". *Arch. Int. Physiol. Biochim.* **81**, 393–394 (1973).
- Storz, G. An Expanding Universe of Noncoding RNAs. *Science* **296**, 1260–1263 (2002).
- Repoila, F., Majdalani, N. & Gottesman, S. Small non-coding RNAs, co-ordinators of adaptation processes in *Escherichia coli*: the RpoS paradigm. *Mol. Microbiol.* **48**, 855–861 (2003).
- Storz, G., Opdyke, J.A. & Zhang, A. Controlling mRNA stability and translation with small, noncoding RNAs. *Curr. Opin. Microbiol.* **7**, 140–144 (2004).
- Valentin-Hansen, P., Eriksen, M. & Udesen, C. The bacterial Sm-like protein Hfq: a key player in RNA transactions. *Mol. Microbiol.* **51**, 1525–1533 (2004).
- Sledjeski, D.D., Whitman, C. & Zhang, A. Hfq is necessary for regulation by the untranslated RNA DsrA. *J. Bacteriol.* **183**, 1997–2005 (2001).
- Sonnleitner, E. *et al.* Reduced virulence of a hfq mutant of *Pseudomonas aeruginosa* O1. *Microb. Pathog.* **35**, 217–228 (2003).
- Majdalani, N., Cunniff, C., Sledjeski, D., Elliott, T. & Gottesman, S. DsrA RNA regulates translation of RpoS message by an anti-antisense mechanism, independent of its action as an antisilencer of transcription. *Proc. Natl. Acad. Sci. USA* **95**, 12462–12467 (1998).
- Lease, R.A., Cusick, M.E. & Belfort, M. Riboregulation in *Escherichia coli*: DsrA RNA acts by RNA:RNA interactions at multiple loci. *Proc. Natl. Acad. Sci. USA* **95**, 12456–12461 (1998).
- Altuvia, S., Zhang, A., Argaman, L., Tiwari, A. & Storz, G. The *Escherichia coli* OxyS regulatory RNA represses *hflA* translation by blocking ribosome binding. *EMBO J.* **17**, 6069–6075 (1998).
- Argaman, L. & Altuvia, S. *hflA* repression by OxyS RNA: kissing complex formation at two sites results in a stable antisense–target RNA complex. *J. Mol. Biol.* **300**, 1101–1112 (2000).
- Zhang, A. *et al.* The OxyS regulatory RNA represses *rpoS* translation and binds the Hfq (HF-I) protein. *EMBO J.* **17**, 6061–6068 (1998).
- Majdalani, N., Chen, S., Murrow, J., St John, K. & Gottesman, S. Regulation of RpoS by a novel small RNA: the characterization of RprA. *Mol. Microbiol.* **39**, 1382–1394 (2001).
- Masse, E. & Gottesman, S. A small RNA regulates the expression of genes involved in iron metabolism in *Escherichia coli*. *Proc. Natl. Acad. Sci. USA* **99**, 4620–4625 (2002).
- Masse, E., Escorcio, F.E. & Gottesman, S. Coupled degradation of a small regulatory RNA and its mRNA targets in *Escherichia coli*. *Genes Dev.* **17**, 2374–2383 (2003).
- Vecerek, B., Moll, I., Afonyushkin, T., Kaberdin, V. & Blasi, U. Interaction of the RNA chaperone Hfq with mRNAs: direct and indirect roles of Hfq in iron metabolism of *Escherichia coli*. *Mol. Microbiol.* **50**, 897–909 (2003).
- Moller, T., Franch, T., Udesen, C., Gerdes, K. & Valentin-Hansen, P. Spot 42 RNA mediates discoordinate expression of the *E. coli* galactose operon. *Genes Dev.* **16**, 1696–1706 (2002).
- Hajnsdorf, E. & Regnier, P. Host factor Hfq of *Escherichia coli* stimulates elongation of poly(A) tails by poly(A) polymerase I. *Proc. Natl. Acad. Sci. USA* **97**, 1501–1505 (2000).
- Le Derout, J. *et al.* Hfq affects the length and the frequency of short oligo(A) tails at the 3' end of *Escherichia coli* *rpsO* mRNAs. *Nucleic Acids Res.* **31**, 4017–4023 (2003).
- Vytvytska, O., Moll, I., Kaberdin, V.R., von Gabain, A. & Blasi, U. Hfq (HF1) stimulates *ompA* mRNA decay by interfering with ribosome binding. *Genes Dev.* **14**, 1109–1118 (2000).
- Folichon, M. *et al.* The poly(A) binding protein Hfq protects RNA from RNase E and exoribonucleolytic degradation. *Nucleic Acids Res.* **31**, 7302–7310 (2003).
- Arluison, V. *et al.* Structural modelling of the Sm-like protein Hfq from *Escherichia coli*. *J. Mol. Biol.* **320**, 705–712 (2002).
- Moller, T. *et al.* Hfq: a bacterial Sm-like protein that mediates RNA–RNA interaction. *Mol. Cell* **9**, 23–30 (2002).
- Zhang, A., Wassarman, K.M., Ortega, J., Steven, A.C. & Storz, G. The Sm-like Hfq protein increases OxyS RNA interaction with target mRNAs. *Mol. Cell* **9**, 11–22 (2002).
- Sun, X., Zhulin, I. & Wartell, R.M. Predicted structure and phyletic distribution of the RNA-binding protein Hfq. *Nucleic Acids Res.* **30**, 3662–3671 (2002).
- Sauter, C., Basquin, J. & Suck, D. Sm-like proteins in eubacteria: the crystal structure of the Hfq protein from *Escherichia coli*. *Nucleic Acids Res.* **31**, 4091–4098 (2003).
- Marchler-Bauer, A. *et al.* CDD: a curated Entrez database of conserved domain alignments. *Nucleic Acids Res.* **31**, 383–387 (2003).
- Schumacher, M.A., Pearson, R.F., Moller, T., Valentin-Hansen, P. & Brennan, R.G. Structures of the pleiotropic translational regulator Hfq and an Hfq–RNA complex: a bacterial Sm-like protein. *EMBO J.* **21**, 3546–3556 (2002).
- Kambach, C. *et al.* Crystal structures of two Sm protein complexes and their implications for the assembly of the spliceosomal snRNPs. *Cell* **96**, 375–387 (1999).
- Achsel, T. *et al.* A doughnut-shaped heteromer of human Sm-like proteins binds to the 3'-end of U6 snRNA, thereby facilitating U4/U6 duplex formation *in vitro*. *EMBO J.* **18**, 5789–5802 (1999).
- Achsel, T., Stark, H. & Luhrmann, R. The Sm domain is an ancient RNA-binding motif with oligo(U) specificity. *Proc. Natl. Acad. Sci. USA* **98**, 3685–3689 (2001).

33. Toro, I. *et al.* RNA binding in an Sm core domain: X-ray structure and functional analysis of an archaeal Sm protein complex. *EMBO J.* **20**, 2293–2303 (2001).
34. Toro, I., Basquin, J., Teo-Dreher, H. & Suck, D. Archaeal Sm proteins form heptameric and hexameric complexes: crystal structures of the Sm1 and Sm2 proteins from the hyperthermophile *Archaeoglobus fulgidus*. *J. Mol. Biol.* **320**, 129–142 (2002).
35. Moll, I., Leitsch, D., Steinhauser, T. & Blasi, U. RNA chaperone activity of the Sm-like Hfq protein. *EMBO Rep.* **4**, 284–289 (2003).
36. Geissmann, T.A. & Touati, D. Hfq, a new chaperoning role: binding to messenger RNA determines access for small RNA regulator. *EMBO J.* **23**, 396–405 (2004).
37. Brescia, C.C., Mikulecky, P.J., Feig, A.L. & Sledjeski, D.D. Identification of the Hfq binding site on DsrA RNA: Hfq binds without altering DsrA secondary structure. *RNA* **9**, 33–43 (2003).
38. Moll, I., Afonyushkin, T., Vytvytska, O., Kabardin, V.R. & Blasi, U. Coincident Hfq binding and RNase E cleavage sites on mRNA and small regulatory RNAs. *RNA* **9**, 1308–1314 (2003).
39. Stage-Zimmermann, T.K. & Uhlenbeck, O.C. Hammerhead ribozyme kinetics. *RNA* **4**, 875–889 (1998).
40. Plum, G.E. & Breslauer, K.J. Calorimetry of proteins and nucleic acids. *Curr. Opin. Struct. Biol.* **5**, 682–690 (1995).
41. Ladbury, J.E. & Chowdhry, B.Z. Sensing the heat: the application of isothermal titration calorimetry to thermodynamic studies of biomolecular interactions. *Chem. Biol.* **3**, 791–801 (1996).
42. Leavitt, S. & Freire, E. Direct measurement of protein binding energetics by isothermal titration calorimetry. *Curr. Opin. Struct. Biol.* **11**, 560–566 (2001).
43. de Haseth, P.L. & Uhlenbeck, O.C. Interaction of *Escherichia coli* host factor protein with oligoriboadenylates. *Biochemistry* **19**, 6138–6146 (1980).
44. Sledjeski, D.D., Gupta, A. & Gottesman, S. The small RNA, DsrA, is essential for the low temperature expression of RpoS during exponential growth in *Escherichia coli*. *EMBO J.* **15**, 3993–4000 (1996).
45. Guzman, L.M., Belin, D., Carson, M.J. & Beckwith, J. Tight regulation, modulation, and high-level expression by vectors containing the arabinose PBAD promoter. *J. Bacteriol.* **177**, 4121–4130 (1995).
46. Mura, C., Kozhukhovskiy, A., Gingery, M., Phillips, M. & Eisenberg, D. The oligomerization and ligand-binding properties of Sm-like archaeal proteins (SmAPs). *Protein Sci.* **12**, 832–847 (2003).
47. Thore, S., Mayer, C., Sauter, C., Weeks, S. & Suck, D. Crystal structures of the *Pyrococcus abyssi* Sm core and its complex with RNA: common features of RNA-binding in Archaea and Eukarya. *J. Biol. Chem.* **278**, 1239–1247 (2003).
48. Urlaub, H., Raker, V.A., Kostka, S. & Luhrmann, R. Sm protein-Sm site RNA interactions within the inner ring of the spliceosomal snRNP core structure. *EMBO J.* **20**, 187–196 (2001).
49. Stark, H., Dube, P., Luhrmann, R. & Kastner, B. Arrangement of RNA and proteins in the spliceosomal U1 small nuclear ribonucleoprotein particle. *Nature* **409**, 539–542 (2001).
50. Arluison, V. *et al.* The C-terminal domain of *Escherichia coli* Hfq increases the stability of the hexamer. *Eur. J. Biochem.* **271**, 1258–1265 (2004).
51. Stoscheck, C.M. Quantitation of protein. *Methods Enzymol.* **182**, 50–68 (1990).
52. Mikulecky, P.J., Takach, J.C. & Feig, A.L. Entropy-driven folding of an RNA helical junction: an isothermal titration calorimetric analysis of the hammerhead ribozyme. *Biochemistry* **43**, 5870–5881 (2004).
53. Schagger, H. & von Jagow, G. Tricine-sodium dodecyl sulfate-polyacrylamide gel electrophoresis for the separation of proteins in the range from 1 to 100 kDa. *Anal. Biochem.* **166**, 368–379 (1987).
54. Towbin, H., Staehelin, T. & Gordon, J. Electrophoretic transfer of proteins from polyacrylamide gels to nitrocellulose sheets: procedure and some applications. *Proc. Natl. Acad. Sci. USA* **76**, 4350–4354 (1979).
55. Brescia, C.C., Kaw, M.K. & Sledjeski, D.D. The DNA binding protein H-NS binds to and alters the stability of RNA in vitro and in vivo. *J. Mol. Biol.* **339**, 505–514 (2004).
56. Bernstein, J.A., Khodursky, A.B., Lin, P.H., Lin-Chao, S. & Cohen, S.N. Global analysis of mRNA decay and abundance in *Escherichia coli* at single-gene resolution using two-color fluorescent DNA microarrays. *Proc. Natl. Acad. Sci. USA* **99**, 9697–9702 (2002).
57. Miller, J.H. *Experiments in Bacterial Genetics* (Cold Spring Harbor Laboratory, Cold Spring Harbor, New York, 1972).